

Rateless codes performance analysis in correlated channel model for GEO Free Space Optics downlinks

A. Andò, G. Messineo, L. Curcio, S. Mangione, P. Gallo, A. C. Busacca

Department of Electrical, Electronic and Telecommunications Engineering, of Chemicals technologies, Automatic Engineering and Mathematical models (DIEETCAM)

University of Palermo

Palermo, Italy

{andrea.ando,alessandro.busacca}@unipa.it

Abstract— Attenuation and fading events can corrupt Free Space Optical (FSO) links. It would be so recommended to add mitigation error codes on the communication links. FSO channel can be described as an *erasure channel* (fading events can cause erasure errors), and we have identified in rateless codes (RCs) a suitable solution to be employed in FSO links. RCs do not need feedback and they add a redundant coding (also tunable on-the-fly as needed) on the source data able to recover the whole payload, despite erasure errors. We implemented two different rateless codes: Luby Transform (LT), Raptor and RaptorQ. We also analyzed code performances on a simulated turbulent GEO FSO downlink (1 Gbps – OOK modulation) at a 1,06 μm wavelength and for different values of zenith angles.

Keywords - *Free Space Optics (FSO); Satellite-to-Ground; correlated channel; Luby Transform (LT) codes; Raptor codes; RaptorQ codes; Fountain codes; rateless codes*

I. INTRODUCTION

Nowadays, Free-space optics (FSO) is a promising technology for broadband communication: its strength is an inexorable, worldwide and ever growing bandwidth demand. In fact, this optical technology offers high bandwidth connectivity and remarkable performances at extremely low costs.

Free-space technology provides wide practical applications for users: optical links have several advantages in comparison with radio links, especially concerning high transmission rates and security. Optical links are used for communication between satellites and/or between satellites and ground stations. Ground stations can be either stationary or mobile: they are placed on building tops, sides and even behind windows, cars and ships.

Digital data is transmitted through the free space, in the baseband, via an intensity-modulated beam of infrared light and processed by optoelectronic devices used in fiberoptic communications. Typically, optical carrier frequencies vary from 200 to 350 THz or equivalent wavelengths ranging from 850 to 1550 nm and are devoid of any license requirements. Moreover, they do not interfere with Satellite broadcasting or other Radio transmission apparatus.

Yet, unfavorable atmospheric conditions strongly influence the transmitted optical signals. Rain, fog, clouds, snow, smog, aerosol scattering and scintillations, inherent to the local weather, and the possible misalignment of receiver and

transmitter due to twisting, swaying and/or bending of structures, create serious difficulties for remote transmissions.

Unfortunately, since the latter processes are non-stationary, i.e. dynamic, they are not easily predictable and, therefore, their influence on an FSO link changes accordingly, with position and time.

Whereas data transmission of ground to satellite FSO communication links is hindered by fluctuations due to atmospheric turbulence, different techniques have been introduced to try to mitigate the effects of signal-intensity fading induced by these. However, regardless of the technique adopted, we recall that an opportune understanding of the propagation properties of laser beams through the atmosphere is fundamental in order to implement a specific mathematical model of a given channel [1-11]. Thus, building a channel model is the first step to develop a tool to simulate the performance of FSO links.

Furthermore, the performance of FSO communication systems can be improved by augmenting the number of both receivers and transmitters [12-14] and by increasing receiver aperture diameter [15].

In this work, we describe the preliminary results of our model of an optical satellite “downlink” to optical ground station implemented to predict the performance of FSO links operating under ‘natural’ weather conditions. We also conducted a series of simulations to fully evaluate its performance, utilizing Luby Transform, Raptor and RaptorQ codes.

II. CHANNEL MODEL

Several impairments afflict FSO links introducing communication problems, as fading and losses. Its intensity is also heavily depending on atmospheric conditions. In our paper we focus on impairments caused by the scintillation phenomena in a Satellite-to-Ground link (Downlink). FSO link apparatus typically exploit tracking systems and so, we considered to be negligible the beam wander effects [16]. Scintillation are due to atmospheric turbulences that originate local variations of the medium refractive index, thus generating optical irradiance fluctuations. In a FSO link the irradiance variations at the receiver can cause both fading losses and erasure errors during communications. In order to investigate about these errors we have designed a simulator which permits

This work is supported by the European Space Agency under grant 5401001020.

us to predict the optical temporal irradiance fluctuations. Specifications of this simulator will describe in the next sessions.

A. Irradiance Probability Distribution Function

Several distribution models were studied in literature to describe optical turbulence effects (e.g. lognormal and negative exponential models) [17-19]. This models are useful to predict specific turbulence conditions such as weak turbulence for lognormal model and very strong turbulence (saturate regime) for negative exponential model. We have chosen a distribution model which allow us to simulate irradiance fluctuations in a large range of turbulence orders. The Gamma-Gamma model [20,21] owns these proprieties and it is very suitable for our studies. In detail, it provides the probability density function (PDF) of optical irradiance values at the receiver and depends on an important parameter: Rytov variance that it can be considered a measure for optical turbulence strength [20]. We can compute the Rytov variance value, for plane wave propagation, as follow:

$$\sigma_I^2 = 2.25\mu_l k^{7/6} (H - h_0)^{5/6} [\sec(\zeta)]^{11/6} \quad (1)$$

where k is wavenumber, H is the satellite altitude, h_0 is ground station altitude, ζ is zenith angle and μ_l is defined as:

$$\mu_l = \int_{h_0}^H C_n^2(h) \left(\frac{h-h_0}{H-h_0} \right)^{5/6} dh \quad (2)$$

C_n^2 [$m^{-2/3}$] is the refractive index structure parameter and its value is variable with altitude. For horizontal paths we can consider it constant. Instead, keeping into account satellite-to-ground communications, it is mandatory to employ a function which describes how C_n^2 changes with altitude. Hufnagel-Valley model [20] is suitable for this purpose and is described by:

$$C_n^2(h) = 0.00594(v/27)^2 (10^{-5}h)^{10} \exp(-h/1000) + 2.7 \times 10^{-16} \exp(-h/1500) + A \exp(-h/100) \quad (3)$$

where v is wind speed and A [$m^{-2/3}$] is a nominal value of C_n^2 at the ground ($C_n^2(0)$).

We simulate a downlink between a geostationary orbit (GEO) satellite and a terrestrial ground station. In this type of link the turbulence path length increases with the link zenith angle, consequently, also optical turbulence effects augment at the receiver. So we compute the Rytov variance values for different zenith angles at the conditions depict in Tab. 1. Results, reported in Tab. 2, show that Rytov variance values are greater than one (under strong atmospheric turbulent conditions) at zenith angle greater than or equal to about 73.8° and less than one (weak turbulence conditions) otherwise.

Starting from the computed Rytov variance values, we are able to produce Gamma-Gamma PDFs using the following expression:

$$p(I) = \frac{2(\alpha\beta)^{(\alpha+\beta)/2}}{\Gamma(\alpha)\Gamma(\beta)} I^{\{[(\alpha+\beta)/2]-1\}} K_{\alpha-\beta}(2\sqrt{\alpha\beta}I) \quad (4)$$

TABLE I. RYTOV VARIANCE COMPUTATION PARAMETERS

Parameters	Value
λ	1.06 nm
v	21 m/s
H	35800 m
h_0	0 m
A	$1,7 \times 10^{-14} m^{-2/3}$

TABLE II. RYTOV VARIANCE AT DIFFERENT VALUE OF ZENITH ANGLE FOR A GEO SATELLITE TO GROUND LINK

Zenith Angle	Rytov variance
0°	0.09
45°	0.12
73.8°	1.01
60°	0.18
60°	0.3
80°	2.4

where I is optical irradiance $\Gamma(\cdot)$ is the Gamma function, $K_n(\cdot)$ is the modified Bessel function of the second kind of order n , while α and β are two factors defined by:

$$\alpha = \left\{ \exp \left[\frac{0.49\sigma_I^2}{(1 + 1.11\sigma_I^{12/5})^{7/6}} \right] - 1 \right\}^{-1} \quad (5)$$

$$\beta = \left\{ \exp \left[\frac{0.51\sigma_I^2}{(1 + 0.69\sigma_I^{12/5})^{5/6}} \right] - 1 \right\}^{-1} \quad (6)$$

In Fig. 1 several Gamma-Gamma curves at different Rytov variance values are depicted.

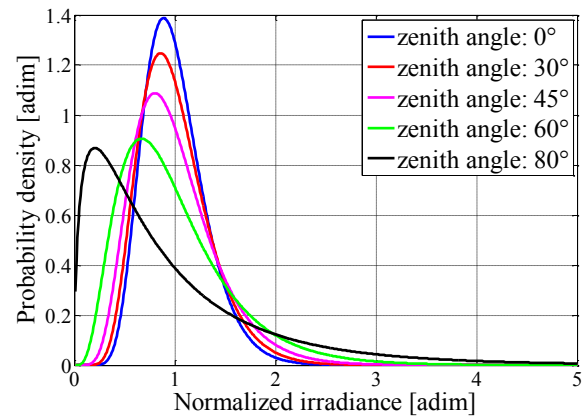


Figure 1. Gamma-Gamma probability density function at different values of zenith angles

As shown, low values of optical irradiance are more probable if the zenith angle increases. Hence, worsening of optical turbulence conditions causes more fading loss events in the FSO channel under study.

B. Irradiance covariance function

In order to predict temporal irradiance fluctuations, we have to define a correlation between irradiance values. For satellite-to-ground downlink plane wave, we can express an irradiance covariance function [21] as follow:

$$B_I(\rho) = \exp \left\{ \begin{array}{l} \sigma_{\ln(x)}^2 [\mu_2(\rho) / \mu_2(0)] + \\ + 0.99 \sigma_{\ln(y)}^2 \left(\frac{k\rho^2 \eta_y}{L} \right)^{5/12} K_{5/6} \left(\sqrt{\frac{k\rho^2 \eta_y}{L}} \right) \end{array} \right\} - 1 \quad (7)$$

where $\sigma_{\ln(x)}$, $\sigma_{\ln(y)}$ and η_y are parameters depending on the Rytov variance, while $\mu_2(\cdot)$ is a function of H , h_0 and C_n^2 .

Previously expression is a function of spatial variable ρ . Under Taylor's *frozen eddies hypothesis* [11, 20,21] we have:

$$\rho = V_T t \quad (8)$$

where t is the time and V_T is the average transverse wind speed (orthogonal to the propagation direction). Thus, we are able to convert the spatial covariance into a time function by setting the V_T in expression (8), and substituting it into (7). The irradiance covariance becomes a function of the only independent variable t and, for this reason, also suitable for our purposes. In order to simulate our channel, we chose $V_T=1\text{m/s}$, obtaining irradiance correlation times close to those experimentally and theoretically reported in literature [22,23].

C. Irradiance fluctuation simulations

In order to predict irradiance fluctuation, at different turbulence conditions, we can generate irradiance time series using the PDF of expression (4) and the temporal covariance of expression (8). Unfortunately, when we try to correlate a non-Gaussian distribution using only a correlation filter, the output distribution converts into a Gaussian one. However, we overcome this difficulty by means of a suitable algorithm [24] which is characterized by a correlation filter and a nonlinear memory-less block function.

The algorithm input parameters are: double side Fourier Transform of the temporal irradiance covariance -obtained through the FFT of $B_I(t)$ - and a random irradiance sequence that follows a Gamma-Gamma distribution. The temporal spacing between two adjacent samples is the reciprocal of the FFT sampling frequency (f_c). We can, at this point, choose the time series resolution according to our needs.

An example of irradiance fluctuation simulation for a GEO satellite downlink with 60° zenith angle, $1.06 \mu\text{m}$ wavelength, $h_0=0$ m, 0.2 s time interval and $10 \mu\text{s}$ time spacing is depicted in Fig. 2.

We also show in Fig. 3 and Fig. 4 a comparison between the input (solid line) statistic sample distributions and temporal covariance function and the output (dashed line) one extracted from the simulated irradiance sequence of irradiance.

The irradiance covariance functions own a plateau that has been considered during simulation procedures and not showed in Fig. 4.

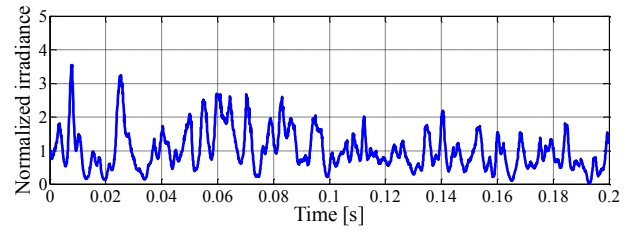


Fig. 2 - Simulated irradiance fluctuations for 60° zenith angle, at 60° zenith angle, $1.06 \mu\text{m}$ wavelength, $h_0=0$ m, 0.2 s time interval and $10 \mu\text{s}$ time spacing.

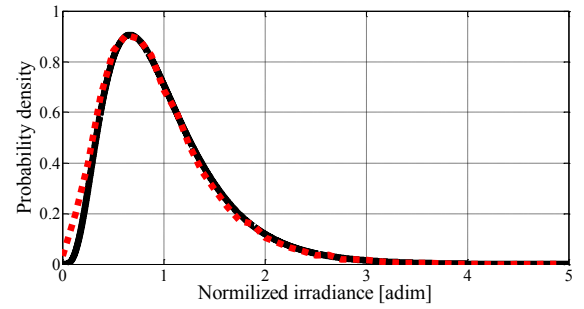


Fig. 3 - Probability Density Function for 60° zenith angle: Theoretical and Simulated irradiance samples sequence.

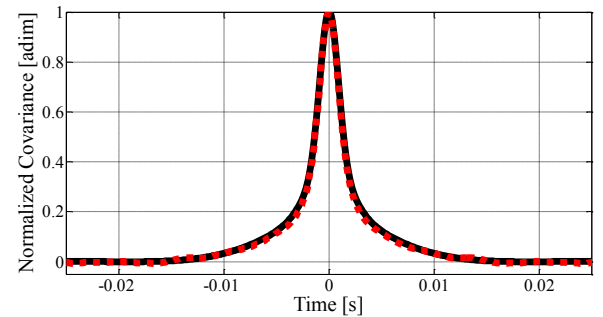


Fig. 4 - Irradiance covariance function for 60° zenith angle: input and simulated irradiance sequence covariances.

It is worth noting that the two mentioned input functions are very similar to the output one. Therefore, the channel we have modeled is able to predict, with good approximation, temporal irradiance fluctuations at the receiver.

III. RATELESS CODES AND SIMULATIONS

We focused our studies on erasure errors caused by irradiance fluctuations at the receiver and we tested also rateless codes in order to improve the quality of communications in a GEO downlink at 1Gbps for different values of zenith angles. The configurations of the simulated link are reported in Tab. 1.

A. Fading statistics

When received optical irradiance falls down a specific threshold, the receiver is not able to distinguish between noise and useful signal. In these cases, the link will suffer an outage that will cause some erasure errors (depending on the outage duration).

Using the above mentioned channel model, we have performed simulation sessions in order to produce fading statistics. Afterward, we compared the results to the theoretical analysis.

In detail, we extracted from the simulated time series, the following three parameters: probability of fade, expected number of fades and mean fade time. From literature [21] we can define the probability of fade by:

$$Pr(I < I_T) = \int_0^{I_T} p_I(I) dI \tag{9}$$

where I_T is the irradiance threshold (which depends on fading threshold that we have set) and $p_I(I)$ is the PDF (in our case Gamma-Gamma distribution). The expected number of fades (for Gamma-Gamma distribution) is defined by:

$$\begin{aligned} \langle n(I_T) \rangle &= \frac{2\sqrt{2\pi\alpha\beta\nu_0\sigma_I}}{\Gamma(\alpha)\Gamma(\beta)} \left(\frac{\alpha\beta I_T}{\langle I \rangle} \right)^{(\alpha+\beta-1)/2} \times \\ &\times K_{\alpha-\beta} \left(2\sqrt{\frac{\alpha\beta I_T}{\langle I \rangle}} \right) \end{aligned} \tag{10}$$

where ν_0 is “quasifrequency” (set to 550 Hz) and σ_I is a parameter which depends on α and β . The mean fade time is:

$$\langle t(I_T) \rangle = \frac{Pr(I < I_T)}{\langle n(I_T) \rangle} \tag{11}$$

In Tab.3, we reported a comparison between the previous parameters as extracted from simulations and calculated with theoretical relationships.

TABLE III. COMPARISON BETWEEN THEORETICAL METHODS AND SIMULATIONS (CORRELATED MODEL) OF THE PROBABILITY OF FADE

Fade threshold: -6 dB		
Zenith angle	Fade probability [%] (Andrews Model)	Fade probability [%] (Correlated Model)
$\zeta = 0^\circ$	0.0043	0.03
$\zeta = 30^\circ$	0.03	0.15
$\zeta = 45^\circ$	0.24	0.60
$\zeta = 60^\circ$	2.06	3.44
$\zeta = 80^\circ$	18.20	18.69

The all data are comparable. However, at the same conditions we highlight how, with the correlated channel model, we have found less expected number of fades (with a longer duration) than theoretical ones.

The outages in FSO communications produce a packet loss but it is possible to mitigate his influence by using proper codes. Rateless codes were designed for erasure channels and, for this reason, it is interesting to investigate their performance on a FSO channel.

TABLE IV. COMPARISON BETWEEN THEORETICAL METHODS AND SIMULATIONS (CORRELATED MODEL) OF THE EXPECTED NUMBER OF FADES

Fade threshold: -6 dB		
Zenith angle	Expected number of fades (Andrews Model)	Expected number of fades (Correlated Model)
$\zeta = 0^\circ$	0.43	6.02
$\zeta = 30^\circ$	2.65	22.70
$\zeta = 45^\circ$	17.01	44.54
$\zeta = 60^\circ$	114.70	93.64
$\zeta = 80^\circ$	607.20	357.45

TABLE V. COMPARISON BETWEEN THEORETICAL METHODS AND SIMULATIONS (CORRELATED MODEL) OF THE MEAN FADE TIME [ms]

Fade threshold: -6 dB		
Zenith angle	Mean fade time [ms] (Andrews Model)	Mean fade time [ms] (Correlated Model)
$\zeta = 0^\circ$	0.10	0.051
$\zeta = 30^\circ$	0.12	0.066
$\zeta = 45^\circ$	0.14	0.135
$\zeta = 60^\circ$	0.18	0.367
$\zeta = 80^\circ$	0.30	0.523

B. Rateless codes

For a decade now, rateless codes play a prominent position in FSO communications. Rateless codes demonstrate their capacity to effectively approach and adapt to any channel, even those with unknown statistics. They add to the source digital data a redundant coding (also settable on the fly) that allows the receiver to recover the whole payload, despite possible erasure errors. For these reasons, rateless codes are typically used in broadcast and multicast transmissions. In this paper, we worked with Fountain codes (FCs) which are rateless and suitable for q-ary erasure channel.

In Fountain Codes, a file is divided into K packets and each packet is composed of a whole number of bits. At each clock cycle, labeled by n, the encoder generates K random bits. Random linear FCs for a group of K packets produce a new set of N packets. FCs perform a linear combination (bitwise sum, modulo-2) of the K source packets by means of a binary pseudo-random G matrix (K x N). Each generated packet will be linked to one or more source packets and the number of such links is termed “degree” (δ). If $N < K$, the receiver has poor information to be able to recover the file; If $N = K$, the receiver has 0.289 probability to recover the file, while If $N > K$, the receiver can recover the file if and only if invertible G

matrix exists, so that the receiver can compute G^{-1} and recover [25].

The G matrix depends on the distribution degrees and its definition is fundamental for the code implementation. We note that LT codes are more efficient than random linear FCs. In order to complete the decoding process, LT codes require two conditions: receiving a number of coded packets $O > K$ and having, for each decoding step, a coded packet with degree equal to 1.

Furthermore, LT codes use a "robust soliton distribution" [25], which offers, at the same overhead, a higher probability to complete the decoding process if compared to the "ideal soliton distribution". In fact, RC are a special case of LT codes and include a pre-coding in order to reduce the expected degree.

Whereas it is possible to improve their computational performances by means of a proper management of sparse graphs. Nevertheless, the degrees distribution does not always guarantee a coding sparse graph and, therefore, a effective decoding speed. However, RC show an expected degree equal to three and, for this reason, the decoding graph is always sparse. Thus, the decoding computational costs are significantly reduced.

Moreover, RC are "systematic codes" and they operate on Galois Field 2 (GF(2)). Nevertheless the number of source symbols is limited to 8192 [26]. RQ codes can be thought as an evolution of RC. They are also "systematic codes" but they work on a much larger alphabet, in particular on GF(256). The use of a larger alphabet reduces the failure probability at a specific overhead. Thus, RQ codes demonstrate better recovering capability. RQ codes permit to find easily good systematic indices [25] using a large number of source symbols.

C. Performance tests

We test all rateless codes mentioned in previous section on OOK 1 Gbps GEO satellite-to-ground downlink with 1518 byte frame size at -6 dB fade threshold and at different values of the zenith angle.

In Fig. 5 and Fig. 6 are shown results of LT codes performance analysis. For all curves we note that over around a 20% of overhead, LT codes have a better recover capabilities. We have found better performances using Raptor and RaptorQ codes. In Fig. 7-8 and Fig 9 are depicted outcome performance tests of Raptor and RaptorQ codes, respectively, at 60° and 80° zenith angles corresponding to an high strength optical turbulence. These results show that RaptorQ have a recover capabilities slightly better than Raptor.

IV. CONCLUSIONS

We produced a FSO channel model that takes into account the temporal covariance of irradiance and hence is able to simulate the temporal irradiance fluctuations at the receiver, with a high resolution. Thanks to this peculiar feature, we can set the temporal spacing among the irradiance time series via a proper sampling frequency for the FFT of the temporal irradiance covariance.

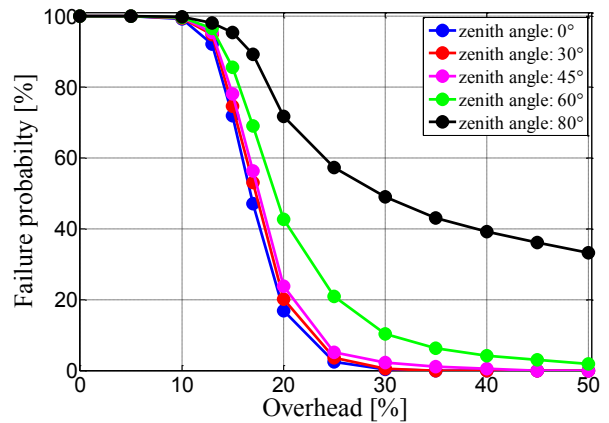


Fig. 5 - LT codes performance for different zenith angle at 1000 K packets and several overhead values

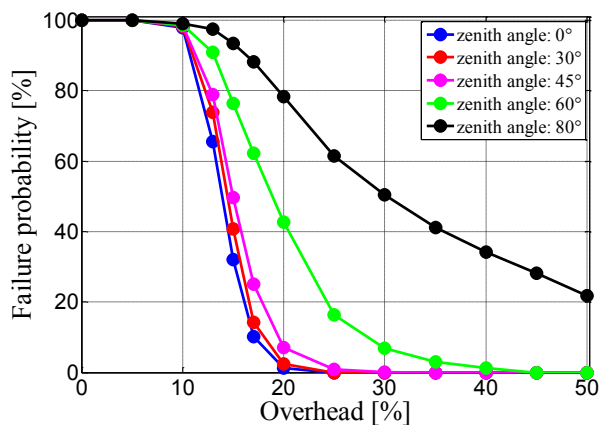


Fig. 6 - LT codes performance for different zenith angle at 2000 K packets and several overhead values

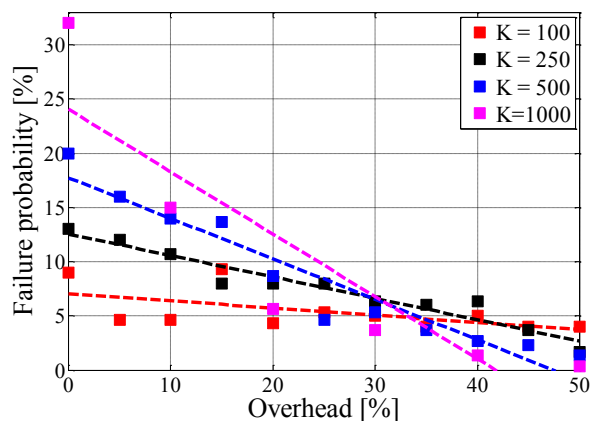


Fig. 7 - Raptor codes performance at 60° zenith angle, different K packets and several overhead values

We also tested, in our channel model, the performances of LT codes and Raptor and RaptorQ codes able to mitigate erasure errors caused by the scintillation phenomena. Our simulations illustrate that LT codes, with K values lower than

2000, are able to cancel erasure errors only for low values of zenith angles.

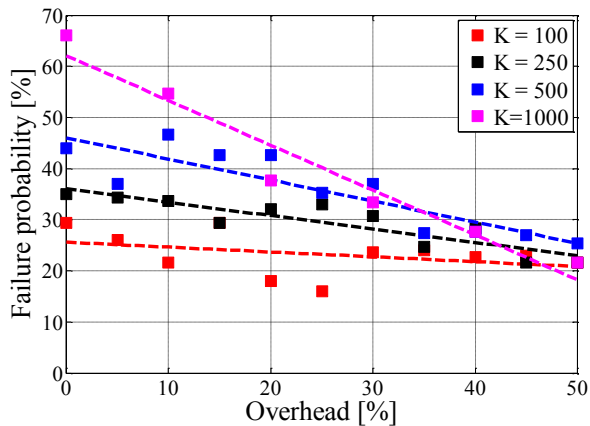


Fig. 8 - Raptor codes performance at 80° zenith angle, different K packets and several overhead values

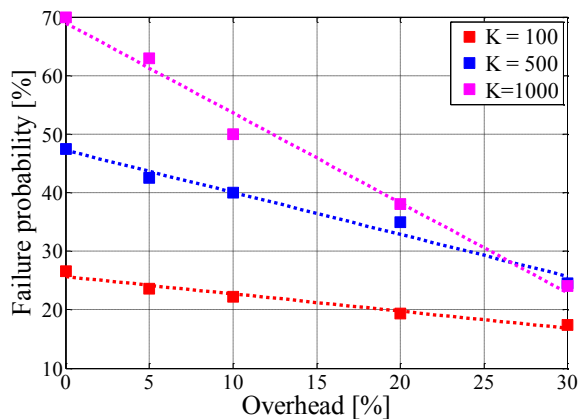


Fig. 9 - RaptorQ codes performance at 80° zenith angle, different K packets and several overhead values

Raptor codes can eliminate erasure errors for 60° zenith angle with an overhead greater than about 40% and at K=1000. Nonetheless, RQ codes provide the best recovering performances. They work slightly better than Raptor and are the best choice especially when high K values are required.

ACKNOWLEDGMENT

We are very grateful to Dr. E. Armandillo for enlightening discussions.

REFERENCES

- [1] V. Chan, "Coding for the turbulent atmospheric optical channel," *IEEE Trans. Commun.*, vol. 30, no. 1, 1982, pp. 269–275.
- [2] Y. T. Koh and F. Davidson, "Interleaved concatenated coding for the turbulent atmospheric direct detection optical communication channel," *IEEE Trans. Commun.*, vol. 37, no. 6, 1989, pp. 648–651.
- [3] J. Li and M. Uysal, "Error performance analysis of coded wireless optical links over atmospheric turbulence channels," in *Proc. IEEE Wireless Commun. Networking Conf. (WCNC)*, Mar. 2004.
- [4] S. Navidpour, M. Uysal, and M. Kavehrad, "Performance bounds for correlated turbulent free-space optical channels," in *Proc. CERS*, Mar. 2006.
- [5] X. Zhu and J. M. Kahn, "Performance bounds for coded free-space optical communications through atmospheric turbulence channels," *IEEE Trans. Commun.*, vol. 51, no. 8, 2003, pp. 1233–1239.
- [6] J. Li and M. Uysal, "Achievable information rate for outdoor free space optical communication with intensity modulation and direct detection," in *Proc. IEEE GLOBECOM*, Nov. 2003, pp. 2654–2658.
- [7] S. Trisno, I. Smolyaninov, S. Milner, and C. C. Davis, "Characterization of time delayed diversity to mitigate fading in atmospheric turbulence channels," *SPIE*, July 2005, pp. 5892151–58921510.
- [8] E. Lee and V. Chan, "Part 1: optical communication over the clear turbulent atmospheric channel using diversity," *IEEE J. Sel. Areas Commun.*, vol. 22, no. 9, pp. 1896–1906, 2004.
- [9] S. Z. Denic, I. Djordjevic, J. Anguita, B. Vasic, and M. A. Neifeld, "Information theoretic limits for free-space optical channels with and without memory," *IEEE J. Lightwave Technol.*, vol. 26, Oct 2008, pp. 3376–3384.
- [10] N. Letzepis and A. G. Fabregas, "Outage probability of the MIMO Gaussian free-space optical channel with PPM," in *Proc. IEEE International Symposium Inf. Theory*, July 2008, pp. 2649–2653.
- [11] S. M. Haas and J. H. Shapiro, "Capacity of wireless optical communications," *IEEE J. Sel. Areas Commun.*, vol. 21, no. 8, 2003, pp. 1346–1357.
- [12] E.J. Lee, V.W.S.Chan, "Optical communications over the clear turbulent channel using diversity," *IEEE Journal on Selected Areas in Communications*, vol. 22, Nov. 2004, pp. 1896–1906.
- [13] S.M.Hass, Capacity of and coding for multiple-aperture, wireless, optical communication, Ph.D. dissertation, Massachusetts Institute of Technology, 2003.
- [14] [14] M. Ali Khalighi, N. Schwartz, N. Aitamer, and S. Bourennane, "Fading reduction by aperture averaging and spatial diversity in optical wireless systems," *Journal of Optical Communication and Networking*, vol. 1, Nov. 2009, pp.580–593.
- [15] L. C. Andrews, R. L. Phillips, and C. Y. Hopen, "Aperture averaging of optical scintillations: power fluctuations and the temporal spectrum," *Waves Random Media*, vol. 10, Jan. 2000, pp. 53–70.
- [16] J.H. Churnside and R.J.Laitaitis, "Wander of an optical beam in the turbulent atmosphere", *Applied Optics* Vol. 29,1990, pp. 926-930.
- [17] S. Karp, R. M. Gagliardi, S. E. Moran, and L. B. Stotts, *Optical Channels: fibers, clouds, water and the atmosphere*. New York: Plenum Press, 1988.
- [18] G. R. Osche, *Optical Detection Theory for Laser Applications*. New Jersey: Wiley, 2002.
- [19] J. W. Goodman, *Statistical Optics*. New York: John Wiley, 1985.
- [20] L. C. Andrews, R. L. Phillips, C. Y. Hopen, "Laser Beam Propagation through Random Media", *Spie Press*, 2005.
- [21] L. C. Andrews, R. L. Phillips, C. Y. Hopen, "Laser Beam Scintillation with Applications", *Spie Press*, 2001.
- [22] J. A. Anguita, M. A. Neifeld, B. Hildner, "Rateless Coding on Experimental Temporally Correlated FSO Channels", *Journal of Lightwave Technology*, Vol. 28, Issue. 7, January 2010, pp. 990 – 1002.
- [23] F. Dios, J. Reolons, A. Rodríguez and O. Batet, "Temporal analysis of laser beam propagation in the atmosphere using computer-generated long phase screens", in *Optics Express*, Vol. 16, Issue 3, 2008, pp. 2206-2220.
- [24] J.M. Nichols, C.C. Olson, J.V. Michalowicz, F. Bucholtz, "A simple algorithm for generating spectrally colored, non-Gaussian signals", *Probabilistic Engineering Mechanics* vol. 25, 2010, pp. 315-322.
- [25] D.J.C. MacKay, "Capacity approaching codes design and implementation - Fountain codes", *IEE Proc.-Commun.*, Vol. 152, no. 6, December 2005, pp. 1062-1068.
- [26] A. Shokrollahi, M.Luby, "Foundations and trends in Communications and Information theory", Vol. 6, no. 3-4, 2011, pp. 213-322.